Sensors and Actuators A 247 (2016) 494–503

Contents lists available at ScienceDirect

Sensors and Actuators A: Physical

journal homepage: www.elsevier.com/locate/sna

Review

Open cracks depth sizing by multi-frequency laser stimulated lock-in thermography combined with image processing

Steve Beuve [a], Zihi Qin [a], Jean-Paul Roger [b,c], Stéphane Holé [a,d,e], Christine Boué [a,d,e,*]

[a] Sorbonne Universités, UPMC Univ Paris 06, F-75005 Paris, France
[b] CNRS, UMR 7587, F-75005, Paris, France
[c] Institut Langevin, PSL Research University, ESPCI ParisTech, 1 rue Jussieu, F-75005, Paris, France
[d] LPEM, PSL Research University, ESPCI-ParisTech, 10 rue Vauquelin, F-75005 Paris, France
[e] CNRS, UMR 8213, F-75005 Paris, France

ARTICLE INFO

Article history:
Received 1 April 2016
Received in revised form 29 May 2016
Accepted 20 June 2016
Available online 1 July 2016

Keywords:
Lock-in
Thermography
Crack depth
Modulation frequency
Infrared images
Non destructive control

ABSTRACT

The multi-frequency lock-in thermography is coupled with efficient image processing to analyse infrared open crack footprint. It has been shown that the evolution of the Laplacian of modulated surface temperature amplitude image as a function of the diffusion length allows to estimate the depth of surface open defects but requires calibration abacus obtained by finite element method simulations. In this work, a method is proposed to avoid the tedious use of abacus by introducing an indicator of the crack depth using a simple expression depending on the Laplacian of both amplitude and phase images. This multi-frequency method is presented through numerical simulations. Besides, the analysis of experimental results obtained on artificial and real open vertical cracks in metallic samples show that the depth of the defects can be directly estimated.

Contents

1. Introduction

Structures submitted to cyclic mechanical loading can develop cracks which can be highly damaging. The depth of a crack is an important information to access its dangerousness. But this information is not easy to obtain. Liquid penetrant, the most conventional method to detect open cracks [1], cannot give worth quantitative information on crack depths. Quantitative estimation

* Corresponding author at: LPEM, PSL Research University, ESPCI-ParisTech, 10 rue Vauquelin, F-75005 Paris, France.
E-mail addresses: jean-paul.roger@espci.fr (J.-P. Roger), stephane.hole@espci.fr (S. Holé), christine.boue@espci.fr (C. Boué).

http://dx.doi.org/10.1016/j.sna.2016.06.028
0924-4247/

can be provided by using methods like ultrasonically stimulated thermography, eddy current stimulated thermography or laser thermographic imaging [2–5]. But these techniques, which are based on the analysis of the generated local rise of the crack temperature, need calibration procedures, a reference response and/or blackened sample to evaluate the crack depth [6–16].

Lock-in thermography uses lateral thermal flows in order to detect vertical cracks [12–15]. The amplitude and phase of infrared images obtained by the diffusion of lateral thermal flows provide information concerning defects with a good contrast for vertical cracks. Ref. [17] proposes an analytical solution of the temperature distribution to deduce the crack width for infinite vertical cracks.

In this work a lock-in thermography procedure is used for depth evaluation of surface-breaking cracks in metals without surface preparation and with no calibration procedure. The implementation of the approach is described in [18–21]: taking advantage of the thermal diffusion length to probe different regions of the sample, the analyse of the amplitude images at the modulation frequency allows to provide crack depth determination but this requires abacus or back simulations to obtain quantitative information. The improvement provided by this work is to process the phase images in addition to the amplitude images to directly allow the determination of depth indicators, avoiding thus the calibration abacus used up to now.

In the first part of this article, the study is led from results of 3D FEM numerical simulations to introduce two depth indicators (μ_A and μ_ϕ) which rely on the evolution of the second spatial derivative of both amplitude and phase images as a function of the thermal diffusion length.

In the second part of this article, experimental results obtained on constant controlled "cracks" in steel and aluminum blocks are analyzed and a global depth indicator I_h calculated from μ_A and μ_ϕ is proposed. Finally, this global indicator I_h is applied to Inconel samples exhibiting real fatigue cracks.

2. Multi-frequency lock-in infrared thermography method

2.1. Principle of the method

The presented method uses a modulated heat excitation associated with lock-in thermography. When a modulated circular laser spot excitation heats the sample surface, the 3D heat transfer equation in solids in the absence of internal heat generation can be used to evaluate the temperature distribution in the whole solid [22]. The lock-in processing of the signals allows a retrieval of both amplitude and phase of the sinusoidal infrared radiation component from the surface sample at the heating fundamental frequency. The unwanted continuous heating (DC) component is thus filtered out.

The second spatial derivatives (Laplacian) of both amplitude and phase images highlight the thermal disturbance caused by the presence of a vertical crack. Crack pixels are extracted from the Laplacian of the amplitude image according to the numerical procedure presented in [23].

In a modulated heating process, the thermal diffusion length, which can be written as

$$\mu = \sqrt{\frac{\alpha}{\pi f}} \tag{1}$$

where α is the thermal diffusivity of the specimen, can be adjusted by the modulation frequency f of the thermal excitation source and used as a 3D probe of the crack depth h. The crack signature is analyzed via the changes of the Laplacian of the amplitude and phase images as a function of the thermal diffusion length μ.

The absolute value of the Laplacian of the amplitude image normalized by its asymptotic value is denoted Λ_N and the value of the Laplacien of the phase image is denoted Λ_ϕ. In [18,19], it is shown that $\Lambda_N(\mu)$ at the crack pixels reach their maximal value at a thermal diffusion length increasing with h and that the evolution of $\Lambda_N(\mu)$ is independent of the crack width. So the evolution of Λ_N with μ is then an indicator of the crack depth. In [19], simulated $\Lambda_N(\mu)$ for various excitation frequencies are used as an abacus to deduce the depth of real cracks. However, these simulations are time consuming (several hours) and must be done for every kind of sample. Besides obtaining the results more quickly, the results do not depend on modelling accuracies. It is thus a great interest to have a direct indicator, independent of the material and its surface condition, to estimate the crack depth.

2.2. Simulated experiments

The objective of this work is to combine the analysis of $\Lambda_N(\mu)$ and $\Lambda_\phi(\mu)$ of crack responses to easily deduce quantitative indicators of the crack depth without any simulation abacus.

The heat source is focused onto the surface in a circular and uniform spot of radius r at a distance d_0 of a linear crack perpendicular to the surface of width w, length L and constant depth h. The heat source is intensity modulated at a frequency f. Amplitude and phase images of the modulated surface temperature at the frequency f are calculated for different h values by 3D FEM numerical simulations. Fig. 1 shows an example of amplitude (Fig. 1a) and phase (Fig. 1b) images of 400*400 pixels (1 pixel sees 50 μm*50 μm) obtained at f = 0.8 Hz. The linear crack footprint is clearly visible in the figures above the heat source. A set of pixels P(x,y) located on the crack which faces the heating zone are extracted from the Laplacian of the amplitude image with a basic numerical processing described in [23] (Fig. 2a). Fig. 2b shows the Laplacian of the phase for these P(x,y) pixels at f = 0.8 Hz. The distance between a pixel P(x,y) and the center of the heating spot is denoted as $d(x,y)$.

2.2.1. One point analysis

The evolution of the Laplacian of the amplitude Λ_N as a function of the thermal diffusion length at the closest pixel P to the heating spot ($d(x,y) = d_0$) is reported in Fig. 3. Simulation results are presented for four depths h as a function of $\mu_i = \sqrt{\alpha/\pi f_i}$ for a frequency ranging from 0.05 Hz to 1.5 Hz.

The polynomial fits $f_h(\mu)$ of $\Lambda_N(\mu_i)$ show a shift along the μ axis which depends on the simulated depth h. Afterward in this work, the value of μ_A corresponding to $f_h(\mu_A) = 0.7$ is then considered as a first indicator for the crack depth evaluation.

The evolution of the absolute value of the Laplacian of the phase images at the same pixel P can also be analyzed. One notices in Fig. 4 that the polynomial fits of simulated $\Lambda_\phi(\mu)$ reach a maximum for $\mu = \mu_\phi$ which is of the order of the crack depth. μ_ϕ is thus retained as a second indicator for the crack depth evaluation.

Fig. 5 shows that the indicator μ_ϕ deduced from the simulations seems to be more dependant on the crack depth h than the indicator μ_A.

2.2.2. Synthesis of crack point analysis

Let's consider the responses of 50 selected pixels on the crack at f = 1.5 Hz. Fig. 6 displays μ_A and μ_ϕ as a function of the distance d between a selected pixel and the center of the heating spot for the four simulated depths h.

One notices in Fig. 6 that μ_A is more d dependant than μ_ϕ. Therefore a combination of μ_A and μ_ϕ is proposed to minimize the influence of d and thus directly estimate the local depth for each selected pixels.

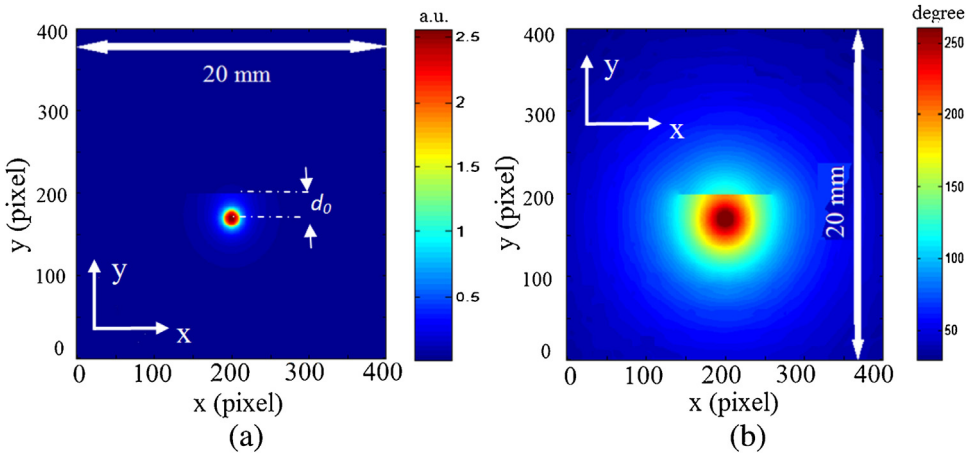

Fig. 1. (a) amplitude image, (b) phase image.
Simulation parameters are $w = 30$ μm, $h = 1$ mm, $L = 6$ mm, $r = 0.5$ mm, $d_0 = 1.5$ mm, $\alpha = 3.3 \times 10^{-6}$ m²/s, $f = 0.8$ Hz. a.u.: arbitrary unit.

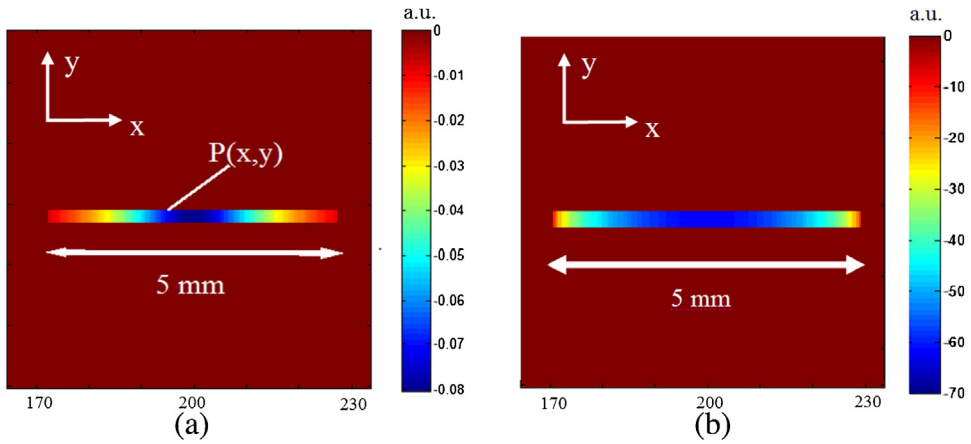

Fig. 2. Pixels P(x,y) extracted from the Laplacian of Fig. 1 images ($f = 0.8$ Hz), (a) Laplacian of the amplitude. (b) Laplacian of the phase. a.u.: arbitrary unit..

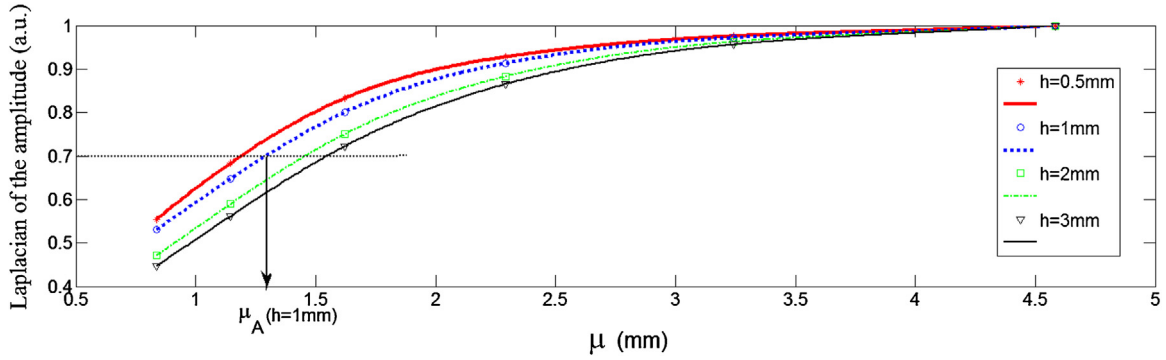

Fig. 3. Simulated $\Lambda_N(\mu_i)$ and polynomial fit $f_h(\mu)$ at the pixel P ($d(x,y) = d_0$) for different depth h.
Simulation parameters are $r = 0.5$ mm, $\alpha = 3.3 \times 10^{-6}$ m²/s, $d_0 = 1.5$ mm, $w = 30$ μm, $L = 6$ mm.

3. Experimental results for the evaluation of the depth

3.1. Experimental set-up and methodology

The experimental set up (Fig. 7) includes a heat source (a diode-pumped Ytterbium laser with 830 nm wavelength and tuneable power), a signal generator which modulates the intensity of the heat source at frequency f, and an infrared camera (Jade III, CEDIP, FLIR). The camera has an array (240*320 pixels) of InSb detectors sensitive in the 3–5 μm wavelength range.

The laser beam is focused onto the surface in the vicinity of the crack in an approximately uniform and circular spot of 1 mm diameter. No surface preparation is required for the studied samples. The laser power is adjusted to the thermal response of the samples.

The generated infrared signals measured by the camera and the reference frequency f are sent to a lock-in detection module (FLIR R9902). The amplitude and phase images of the f-component of the IR emission induced at the surface of the inspected sample is then extracted with a fairly good contrast (Fig. 8a and b).

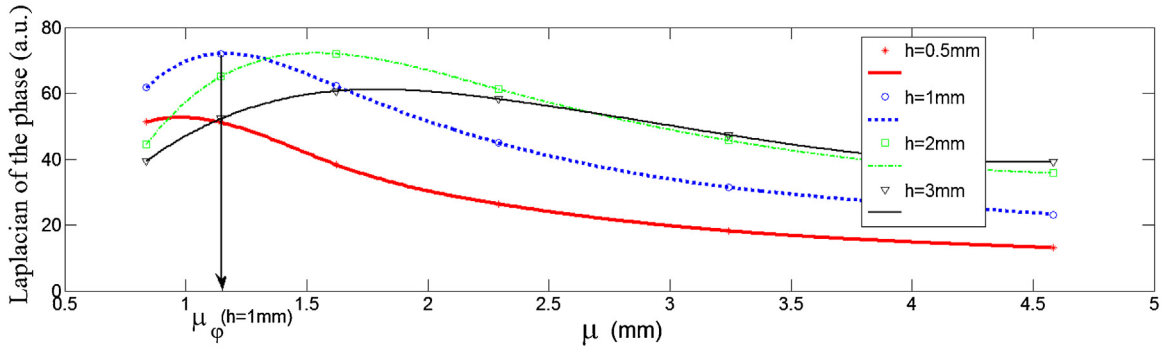

Fig. 4. simulated $\Lambda_\phi(\mu_i)$ and polynomial fits at the pixel P $(d(x,y)=d_0)$ for different depths h.
Simulation parameters are $r=1$ mm, $\alpha=3.3\times10^{-6}$ m^2/s, $d_0=1.5$ mm, $w=30$ μm, $L=6$ mm.

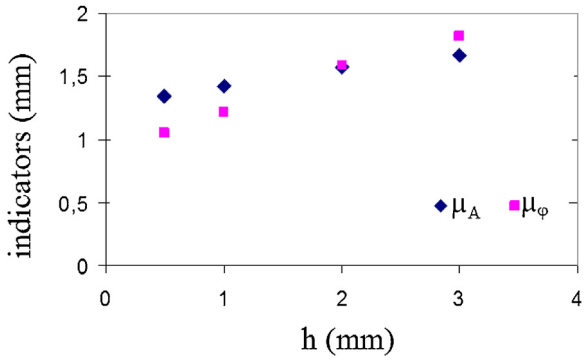

Fig. 5. μ_A and μ_ϕ as a function of simulated depth h at the pixel P $(d(x,y)=d_0)$.

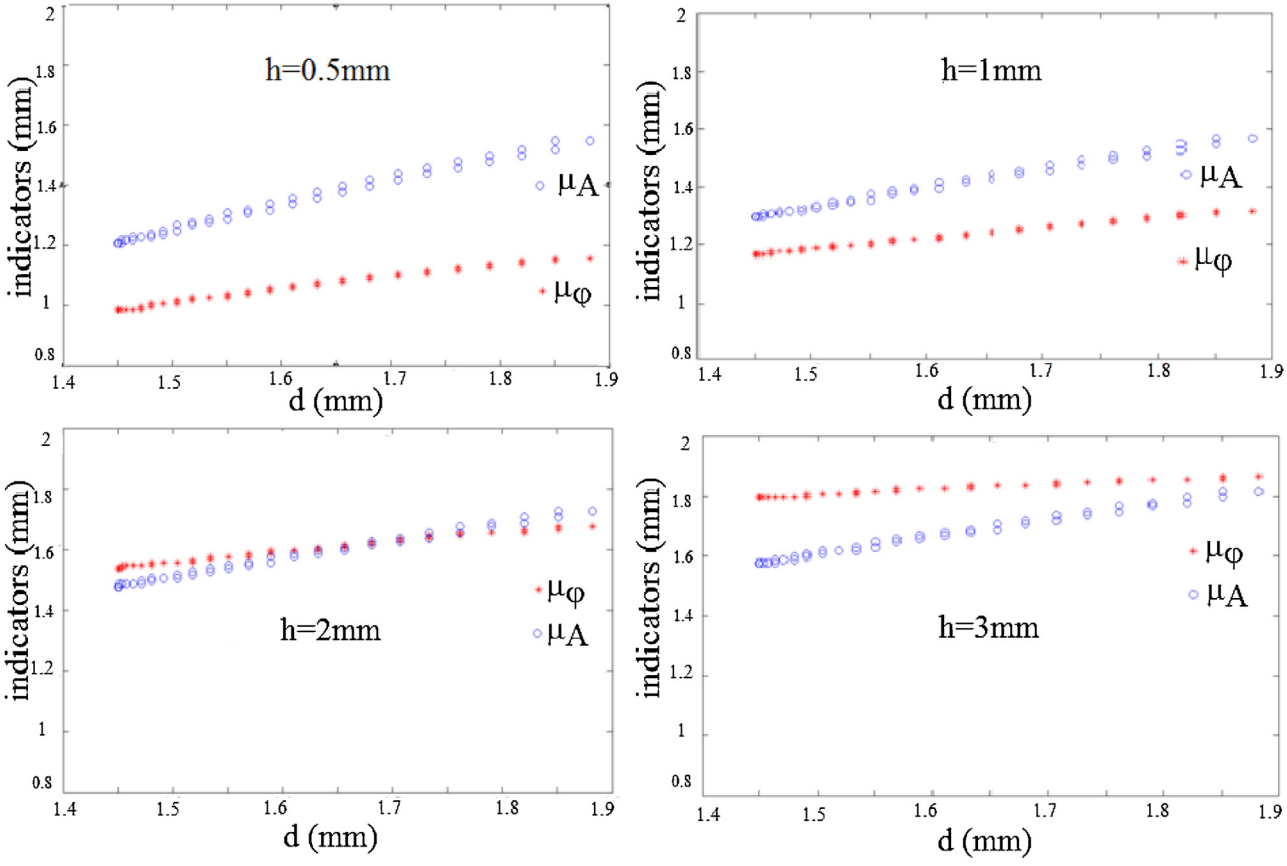

Fig. 6. μ_A and μ_ϕ as a function of the distance d for the 4 simulated depths h.

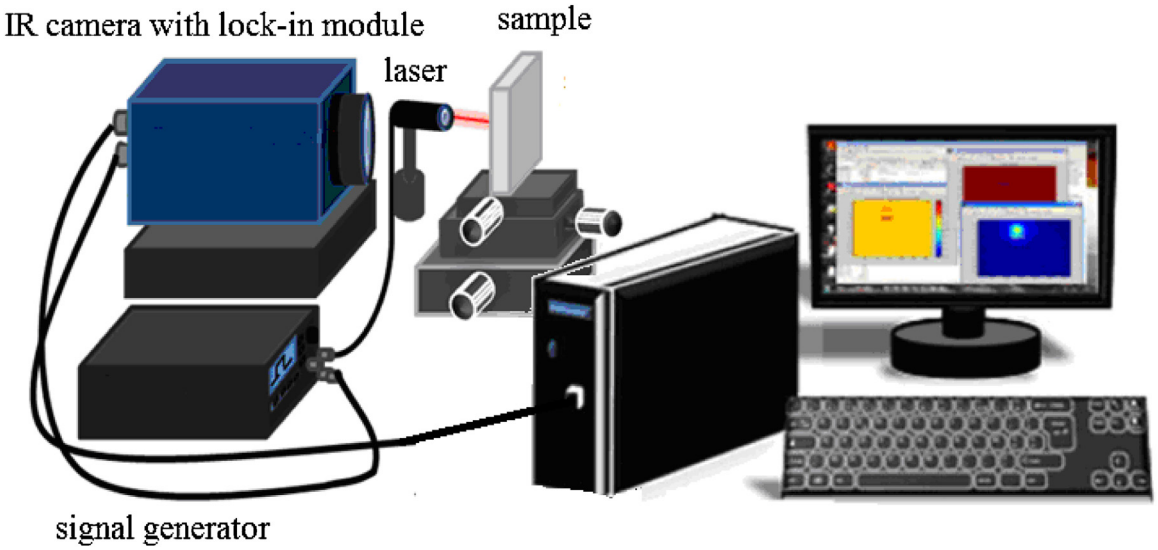

Fig. 7. experimental set-up.

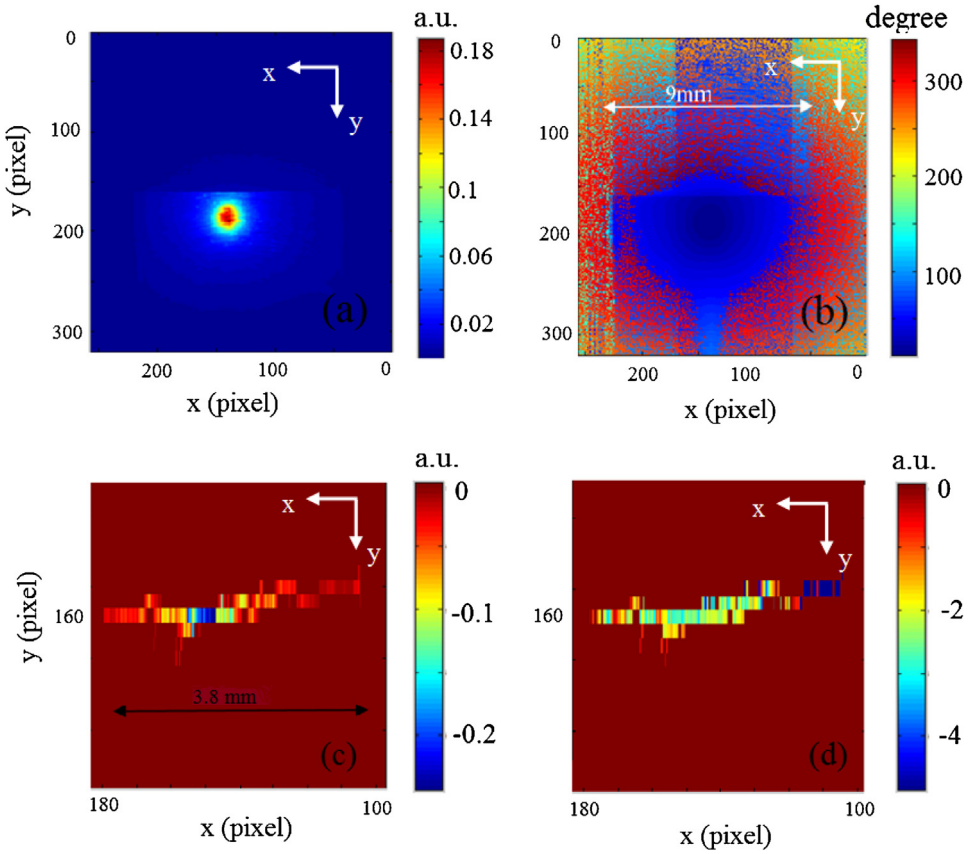

Fig. 8. example of a fatigue crack. (a) Amplitude image, (b) Phase image, (c) Laplacian of the amplitude of the selected P(x,y) pixels calculated using Fig. 8a, (d) Laplacian of the phase for the selected pixels calculated using Fig. 8b. f = 0.05 Hz, 1 pixel corresponds to 50 μm*50 μm. a.u.: arbitrary unit.

The Laplacian of amplitude and phase images (Fig. 8c and d) are proceeded according to the procedure described in the former section to calculate μ_A and μ_ϕ from the polynomial fits of $\Lambda_N(\mu)$ and $\Lambda_\phi(\mu)$ (Fig. 9). Notice that local diffusivity α of each sample can be directly extracted from measurements [24], in a homogeneous area sufficiently far away from the crack.

3.2. Experimental measurements with controlled artificial cracks

Artificial cracks with controlled dimensions are good samples to validate experimentally the simulated results presented in Section 2.

Two 40*40*20 mm^3 steel and aluminum alloy plates separated by a brass sheet of 30 μm thickness are assembled with screws

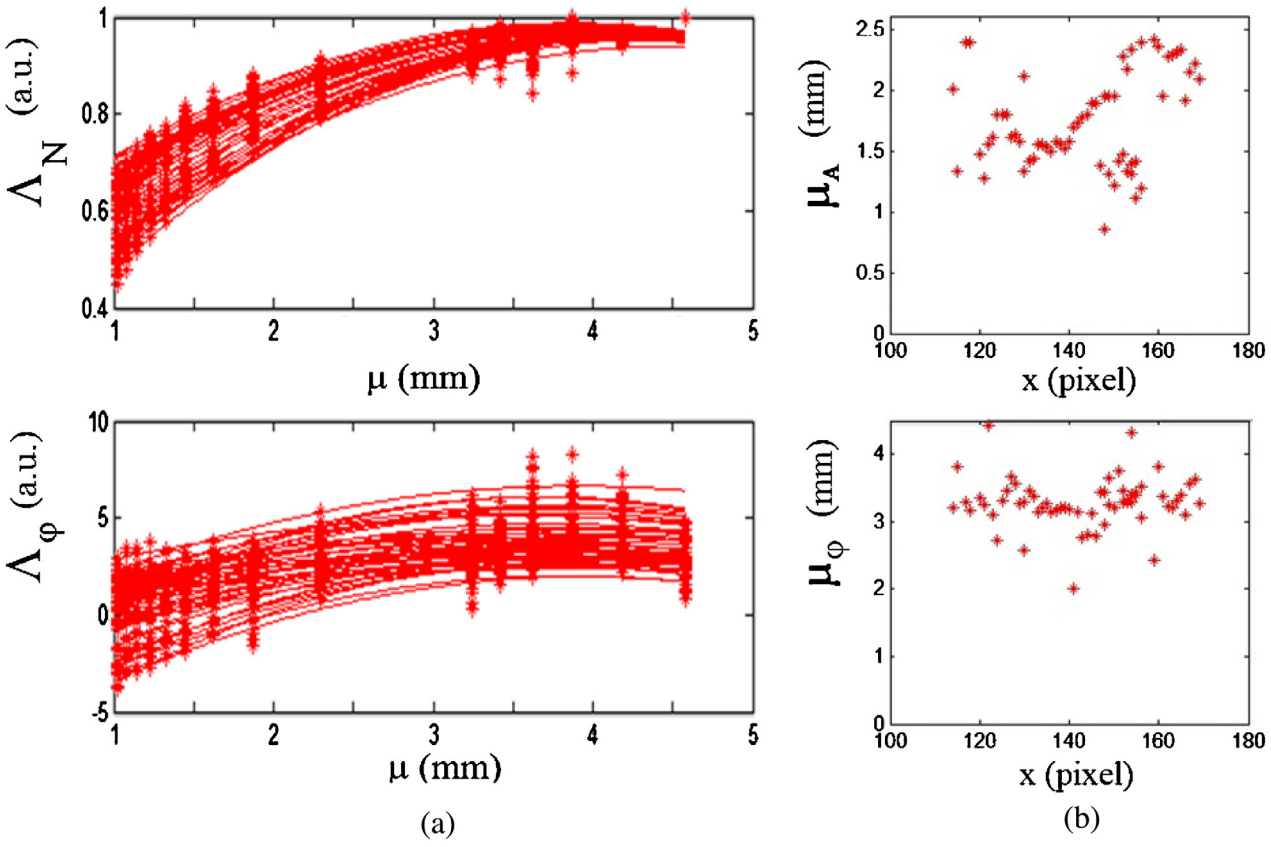

Fig. 9. (a) Experimental Λ_N and Λ_ϕ and polynomial fits as a function of μ for the selected pixels in the sample of Fig. 8. (b) Deduced μ_A and μ_ϕ for the selected pixels along the x direction.
f is varying from 0.05 Hz to 1.5 Hz.

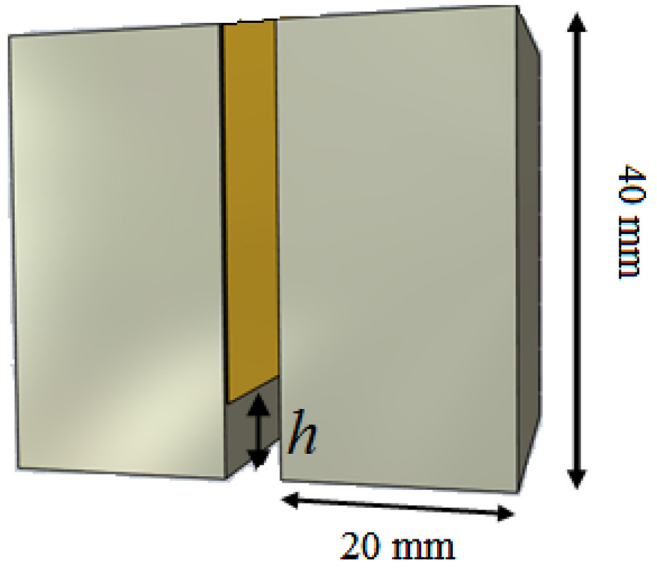

Fig. 10. simulation of a controlled depth crack in a steel or aluminum alloy sample. The brass sheet exhibits a constant h cut.

to simulate a sample with a vertical open crack (Fig. 10). In the presented results, the brass sheet was cut in z direction so as to leave an air gap of controlled constant depth between two steel plates (Samples F, thermal diffusivity equal to $3.7 \pm 0.2 \times 10^{-6}$ m^2/s) or two aluminum alloy blocks (sample G, thermal diffusivity equal to $40 \pm 2 \times 10^{-6}$ m^2/s) as described in Table 1. The laser power is 4 W.

Table 1
crack sizes of steel and aluminum alloy samples.

	Controlled depth h (mm)	crack width (μm) measured by optical microscopy
F1 – steel	0.7 ± 0.1	30 ± 5
G – aluminum alloy	1 ± 0.1	30 ± 5
F2 – steel	1.5 ± 0.1	30 ± 5
F3 – steel	2.5 ± 0.1	30 ± 5

Fig. 11 shows μ_A and μ_ϕ as a function of the distance d obtained for the four studied samples. One can observe that μ_A and μ_ϕ follow the same trends as simulation results (Fig. 6): μ_A and μ_ϕ are both dependant on h and μ_ϕ is less d dependant than μ_A but μ_ϕ is noisier than μ_A in the presented experimental results.

3.3. Global depth indicator

In order to minimize the dependence on d of μ_A and μ_ϕ and to give an enhanced robustness to the depth assessment at each selected pixel, a new depth indicator I_h depending on μ_A, μ_ϕ and d is defined as:

$$I_h(x,y) = \frac{\mu_A(x,y) * \mu_\phi(x,y)}{a * d(x,y)} \quad (2)$$

where a is an adjustment parameter. For depth range from 0.5 mm to 3 mm and for the experimental conditions, $a = 2$ is well adapted as shown hereafter.

Fig. 12 shows the depth indicator I_h obtained with the presented multi-frequency lock-in thermography method using (2) with $a = 2$ for the four samples. The results are presented in x,y plane with

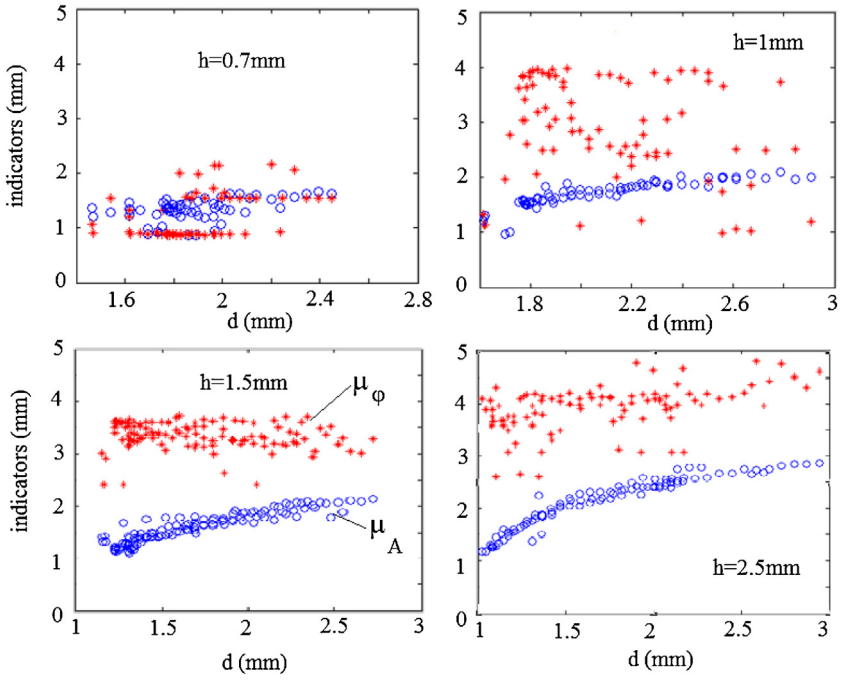

Fig. 11. μ_A (blue circle) and μ_ϕ (red star) responses as a function of distance d for four depth h. (For interpretation of the references to colour in this figure legend, the reader is referred to the web version of this article.)

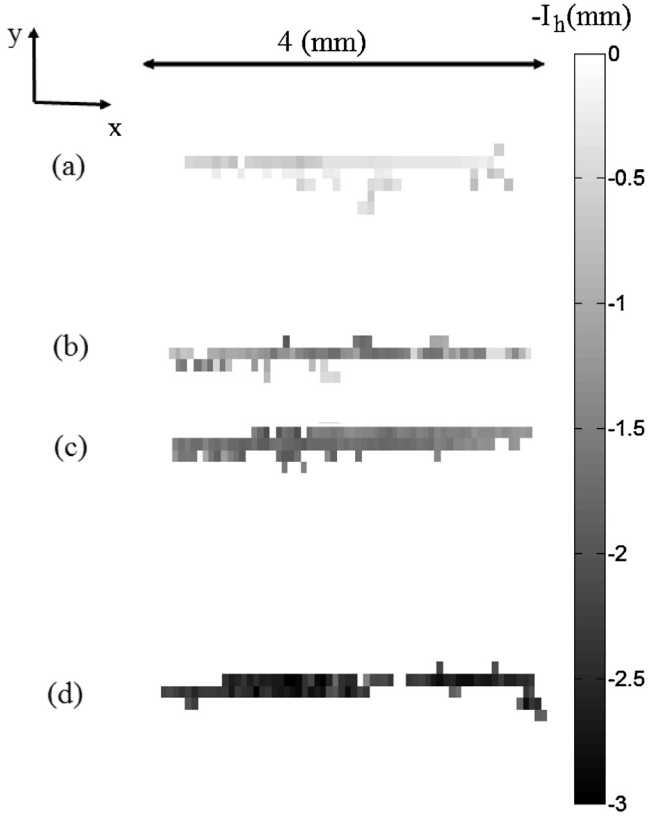

Fig. 12. I_h for the selected pixels in x,y plane. 1 pixel represents 80 μm*80 μm, $a = 2$.
The color indicates (negative) I_h evaluation of each selected pixels. (a) Steel sample F1, expected depth around 0.7 mm, (b) Aluminum alloy sample G, expected depth around 1 mm, (c) Steel sample F2, expected depth around 1.5 mm, (d) steel sample F3, expected depth around 2.5 mm.

the same color scale to give a comparative and visual indication of the depth for each selected pixels of the 4 cracks. The experimental results seem coherent with the expected h values.

Fig. 13 displays the average value over the selected pixels P(x,y) of $\mu A\ (x,y)$, $\mu_\phi\ (x,y)$ and $I_h(x,y)$, respectively denoted as $\tilde{\mu}_A$, $\tilde{\mu}_\phi$ and $\tilde{I}_h$ obtained for the four samples as a function of expected

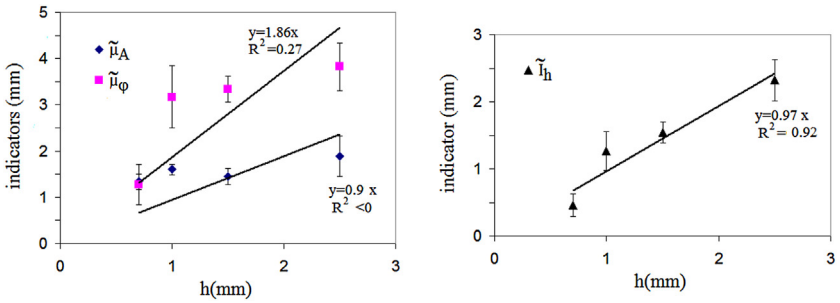

Fig. 13. $\tilde{\mu}_A$, $\tilde{\mu}_\phi$ indicators (left) and $\tilde{I}_h$ indicator (right) as a function of expected h values obtained on the steel and aluminum alloy samples. Estimate slope of linear regression through the origin and R-squared coefficient R^2 are added for each indicators.

depths. Linear regressions through the origin are calculated for the three indicators. The R-squared coefficient R^2 which represents the correlation between the predictive value and the average of the indicators show that $\tilde{I}_h$ indicator is the better indicator (R^2 near 1). The negative R^2 coefficient obtained for $\tilde{\mu}_A$ is nonsense and indicates that the linear fitting through the origin is not appropriate. As μ_A and μ_ϕ are correlated measurements, the error bars of the $\tilde{I}_h$ indicators are smaller than the error bars of $\tilde{\mu}_A$ and $\tilde{\mu}_\phi$ indicators. One can see that the indicator $\tilde{I}_h$ is comparable to the expected depth h, though a bias exists for small depths.

The results validate the method to evaluate constant crack depths within the tested depth range from 0.7 to 2.5 mm.

3.4. Inconel samples with real fatigue cracks

Five open vertical fatigue cracks of 35–65 μm widths in a highly reflecting 130*27*9 mm^3 Inconel plates (samples A–E) are opened over the entire width of the samples. Depths are measured on the 2 lateral sides of the sample using optical microscopy [18] (Table 2). The measured thermal diffusivity of the Inconel sample is equal to $3.3 \pm 0.1 \times 10^{-6}$ m^2/s. The laser power is 2 W.

Fig. 14 shows I_h using (2) with $a = 2$ in (x,y) planes for Inconel samples.

Fig. 15 presents the averaged indicators $\tilde{\mu}_A$, $\tilde{\mu}_\phi$and $\tilde{I}_h$ calculated from selected pixels of the crack as a function of expected averaged depth h. Linear regressions through the origin are calculated for the three indicators. The R-squared coefficient R^2 is nearer to 1 for $\tilde{\mu}_\phi$ than for $\tilde{I}_h$ and has no sense for $\tilde{\mu}_A$. If the result obtained for sample E ($h > 3$ mm) is ignored, the linear regression for $\tilde{I}_h$ gives comparable results to those obtained for steel and aluminum samples (Fig. 13): $R^2 = 0.92$ and $y = 0.92\,x$.

Consequently, $\tilde{I}_h$ seems to be a good direct indicator of the depth h at least for h lesser than 3 mm. Although it seems that the sensitivity of the measurement reaches its limit for Sample E, the proposed multi-frequency lock-in thermography approach appear to be promising to locally probe local crack depth without sample modelling.

4. Conclusion

In this work, the multi-frequency lock-in infrared thermography method is used to evaluate perpendicular crack depths. A specific empirical data analysis is presented using the experimental curves of the spatial second derivative (Laplacian) of both amplitude and phase infrared images as a function of the thermal diffusion length. Two direct depth indicators μ_A and μ_ϕ are introduced and their evolution as a function of the crack depth h and the distance d of the crack to the heating spot are analyzed. A combination of μ_A, μ_ϕ and d is used to make a depth indictor I_h independent of distance

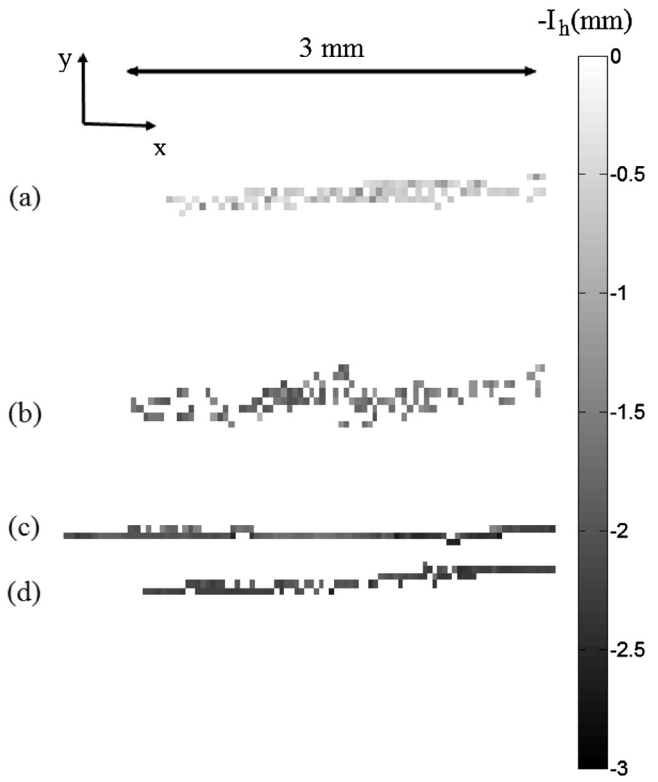

Fig. 14. I_h for the selected pixels as a function of pixel location in (x,y) plane, 1 pixel represents 50 μm*50 μm. (a) Inconel sample A, expected depth around 0.4 mm, (b) Inconel sample B, expected depth around 1.6 mm, (c) Inconel sample D, expected depth around 2.1 mm, (d) Inconel sample E, expected depth around 3.2 mm.

d. It can be seen as a compromise which enhances the robustness of the depth evaluation.

Measurements were carried out on Inconel alloy samples with calibrated 0.5 mm–3.5 mm crack depths. The measurement duration depends on the number of used frequencies. Typically for metals, one can consider 5 different frequencies between 0.05 Hz and 1.5 Hz which lead to 10 min measurement duration. The distance of heat source to the inspected crack and the frequencies selected to probe the volume of the sample must be thoroughly chosen so that the sensibility is optimal. This distance depends on the thermal diffusivity of the sample. The depth range for the studied material is from about 0.5–3 mm.

Acknowledgment

The authors would like to thank Areva Intercontrole for providing Inconel samples with various calibrated fatigue cracks.

Table 2
crack sizes of Inconel alloy samples.

Inconel	Depth (mm) on the two lateral sides of the sample		averaged depth (mm) deduced from the values of the first columns	crack width (μm)
Sample A	0.2 ± 0.1	0.6 ± 0.1	0.4	20 ± 10
Sample B	1 ± 0.1	2.1 ± 0.1	1.6	40 ± 10
Sample C	1.1 ± 0.1	3.1 ± 0.1	2.1	35 ± 5
Sample D	1.7 ± 0.1	2.4 ± 0.1	2.1	65 ± 5
Sample E	2.8 ± 0.1	3.6 ± 0.1	3.2	45 ± 5

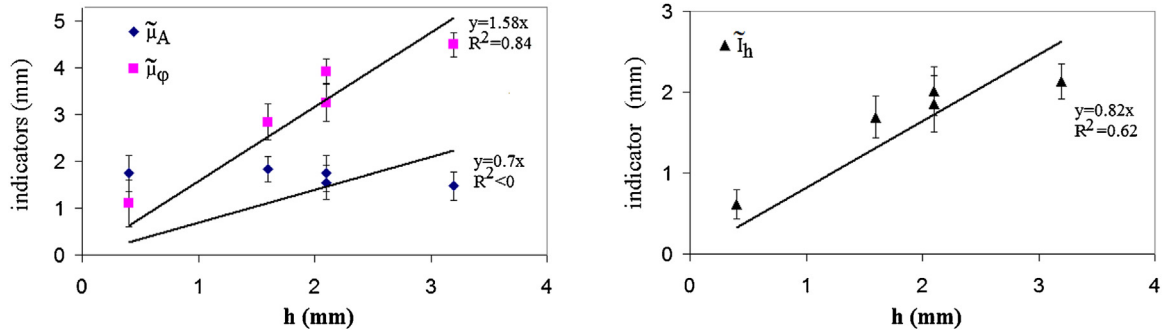

Fig. 15. $\tilde{\mu}_A$, $\tilde{\mu}_\phi$ indicators (left) and $\tilde{I}_h$ indicator (right) as a function of expected h values obtained on the Inconel alloy samples. Estimate slope of linear regression through the origin and R-squared coefficient R^2 are added for each indicators.

References

[1] L. Cartz, Nondestructive Testing, ASM International, Materials Park, Ohio, 1995.
[2] D.P. Almond, B. Weekes, T. Li, S.G. Pickering, E. Kostson, J. Wilson, G.Y. Tian, S. Dixon, S. Burrows, Thermographic techniques for the detection of cracks in metallic components, Insight—Non-Destr. Test. Cond. Monit. 53 (November (11)) (2011) 614–620.
[3] J.-C. Krapez, L. Legrandjacques, F. Lepoutre, D. Balageas, Optimization of the Photothermal Camera of Crack Detection, QIRT 1998 Archives: Documents and Sessions Presented During the 4th Conference on QIRT, Lodz, Poland, 1998.
[4] B.A. Auld, J.C. Moulder, Review of advances in quantitative Eddy current nondestructive evaluation, J. Nondestr. Eval. 18 (1) (1999).
[5] A. Dillenz, T. Zweschper, G. Riegert, G. Busse, Progress in phase angle thermography, Rev. Sci. Instrum. 74 (2003) 417–419.
[6] M. Morbidini, P. Cawley, A calibration procedure for sonic infrared nondestructive evaluation, J. Appl. Phys. 106 (023504) (2009), http://dx.doi.org/10.1063/1.3169518.
[7] B. Weekes, D.P. Almond, P. Cawley, Tim Barden, Eddy-current induced thermography–probability of detection study of small fatigue cracks insteel, titanium and nickel-based super alloy, NDT & E Int. 49 (2012) 47–56.
[8] J. Schlichting, Ch. Maierhofer, M. Kreutzbruck, Crack sizing by laser excited thermography, NDT & E Int. 45 (2012) 133–140.
[9] T. Li, D.P. Almond, S. Rees, Crack imaging by scanning pulsed laser spot thermography, NDT & E Int. 44 (2) (2011) 216–225.
[10] O. Wysocka-Fotek, W. Oliferuk, M. Maj, Reconstruction of size and depth of simulated defects in austenitic steel plate using pulsed infrared thermography, Infrared Phys. Technol. 55 (2012) 363–367.
[11] S. Lugin, Detection of hidden defects by lateral thermal flows, NDT & E Int. 56 (2013) 48–55.
[12] T. Sakagami, S. Kubo, Y. Teshima, Fatigue crack identification using near-tip singular temperature field measured by lock-in thermography, SPIE Proc. Ser. 4020 (2000) 174–181.
[13] C. Wallbrink, S.A. Wade, R. Jones, The effect of size on the quantitative estimation of defect depth in steel structures using lock-in thermography, J. Appl. Phys. 101 (2007) 104907.
[14] M. Choi, K. Kang, J. Park, W. Kim, K. Kim, Quantitative determination of a subsurface defect of reference specimen by lock-in infrared thermography, NDT & E Int. 41 (2008) 119–124.
[15] D. Peng, R. Jones, Lock-in thermographic inspection of squats on rail steel head, Infrared Phys. Technol. 57 (2013) 89–95.
[16] A. Mendioroz, A. Castelo, R. Celorrio, A. Salazar, Characterization of vertical buried defects using lock-in vibrothermography: I. Direct problem, Meas. Sci. Technol. 24 (065601) (2013), 11 pp.
[17] N.W. Pech-May, A. Oleaga, A. Mendioroz, A.J. Omella, R. Celorrio, A. Salazar, Vertical cracks characterization using lock-in thermography: I infinite cracks, Meas. Sci. Technol. 25 (115601) (2014), 10 pp.
[18] M. Streza, Y. Fedala, J.-P. Roger, G. Tessier, C. Boué, Heat transfer modeling for surface crack depth evaluation, Meas. Sci. Technol. 24 (045602) (2013), 6 pp.
[19] Y. Fedala, M. Streza, J.-P. Roger, G. Tessier, C. Boué, Open cracks depth sizing by laser stimulated Infrared lock-in thermography, J. Phys. D: Appl. Phys. 47 (465501) (2014), 6 pp.
[20] C. Boué, G. Tessier, J.-P. Roger, M. Streza, Procédé d'évaluation de la profondeur d'une fissure French Patent Application no 12 58940, PCT/FR2013/052185, CNRS–UPMC, 2013.
[21] C. Boué, G. Tessier, J.-P. Roger, M. Streza, Method for assessing the depth of a crack, US Patent, publication number 2015-0241212, 2015.
[22] H.S. Carslaw, J.C. Jaeger, Conduction of Heat in Solids, 2nd ed., Oxford Press, 1959, 16.
[23] Y. Fedala, M. Streza, F. Sepulveda, J.-P. Roger, G. Tessier, C. Boué, Infrared lock-in thermography crack localization on metallic surfaces for industrial diagnosis, J. Non-Destr. Eval. (2013), http://dx.doi.org/10.1007/s10921-013-0218-4.
[24] C. Boué, S. Holé, Infrared thermography protocol for simple measurements of thermal diffusivity and conductivity, Infrared Phys. Technol. 55 (2012) 376–379.

Biographies

Steve Beuve was student of sensors, instrumentation & mesurements master at Pierre & Marie Curie University, Paris, France.

Zihi Qin was student of sensors, instrumentation & mesurements master at Pierre & Marie Curie University, Paris, France.

Jean Paul Roger is associate professor at the Langevin Institute, ESPCI ParisTech (France). He received the PhD degree in physical sciences from Pierre and Marie Curie University in 1988. His main research fields are: thermal characterization of materials, thin films and structures using optically based photothermal techniques (mirage detection, photoreflectance microscopy, dynamic ellipsometry), and development of interferometric, reflectance and ellipsometric microscopy imaging techniques to measure the displacement fields of actuated micromechanical systems and/or to map films growth.

Stéphane Holé joined Laboratoire d'Électricité Générale of École Supérieure de Physique et de Chimie Industrielles (Paris, France) to study an instrument for measuring fast development of space charges in insulators under rapid voltage variations. It was the topic of his PhD he received in 1996. Currently Professor at Université Pierre et Marie Curie, he leads the Instrumentation Group in Laboratoire de Physique et d'Étude des Materiaux since 2007. His research topics are various such as space charge in insulators and semiconductors (main topic), electrostatic, magnetostatic and ultrasonc sensors. He received the Jack Hollingum Award in 2002 and 2004, and obtained his Habilitation in 2007. He teaches solid state physics, electronics and sensor physics. He is coordinator of the sensors, instrumentation & mesurements master at Pierre & Marie Curie University since 2009.

Christine Boué received her Ph.D. degree in electrical engineering in 1991 from the University Pierre et Marie Curie in association with the Ecole Supérieure de Physique et de Chimie Industrielles, Paris France. During her Ph.D. thesis, she studied the distribution of space charges in piezoelectric polymers. She is currently an Associate Professor at Sorbonne Universités-UPMC (France) since 1992 where she teaches electronics, microcontroller interfacing, signal processing. Her research topics concern thermal imaging and non-destructive testing by synchronous infrared thermography.